THE JOURNAL OF PHYSICAL CHEMISTRY A

ARTICLE

pubs.acs.org/JPCA

# Electron Distribution in Partially Reduced Mixed Metal Oxide Systems: Infrared Spectroscopy of $Ce_mV_nO_o^+$ Gas-Phase Clusters

Ling Jiang,[†] Torsten Wende,[†] Pieterjan Claes,[‡] Soumen Bhattacharyya,[‡] Marek Sierka,[§] Gerard Meijer,[†] Peter Lievens,[*,‡] Joachim Sauer,[*,§] and Knut R. Asmis[*,†]

[†]Fritz-Haber-Institut der Max-Planck-Gesellschaft, Faradayweg 4-6, D-14195 Berlin, Germany

[‡]Laboratory of Solid State Physics and Magnetism, K.U.Leuven, Celestijnenlaan 200 D, B-3001 Leuven, Belgium

[§]Institut für Chemie, Humboldt-Universität Berlin, Unter den Linden 6, D-10099 Berlin, Germany

Supporting Information

**ABSTRACT:** Vibrational predissociation spectra of rare-gas-tagged $[(CeO_2)(VO_2)_{1-2}]^+$ and $[(Ce_2O_3)(VO_2)]^+$ clusters are measured in the 400−1200 $cm^{-1}$ region. Density functional theory (DFT) is used to determine the geometric and electronic structure of low-energy isomers of the partially reduced clusters. Comparison of experimental and simulated spectra provides evidence for the larger stability of $Ce^{+3}/V^{+5}$ compared to that of $Ce^{+4}/V^{+4}$, which confirms that the exceptionally high reducibility of $Ce^{+4}$ accounts for the promoting role of ceria in supported vanadium oxide catalysts.

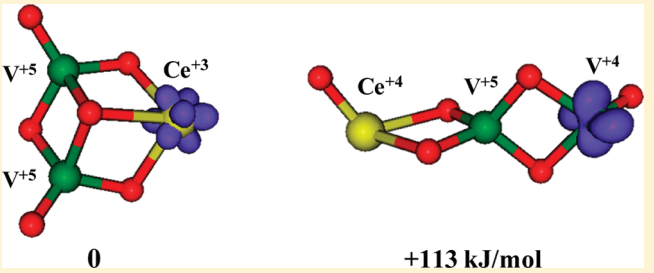




## 1. INTRODUCTION

Supported vanadia is an important solid catalyst for selective oxidations, for example, for the oxidative dehydrogenation (ODH) of alkanes and methanol.[1,2] It has therefore been chosen as a material for examining the role of the supporting oxide on the catalytic activity,[2−5] and a strong dependence on the type of the supporting oxide has been found, the origin of which is still under debate. Among the factors discussed is the reducibility of the support material because hydrogen transfer, the rate-determining step in the ODH reaction,[6−8] leaves an electron on the supported vanadium oxide catalysts. For vanadia supported on ceria, the catalytic activity is particularly high.[2,5,9] Although cerium oxide has been known for its ability to store, release, and transport oxygen ions for a long time,[10] only recently, a combined experimental and computational investigation of $VO_x/CeO_2$-(111) model catalysts has shown that this remarkable activity is due to the ability of ceria to easily accommodate electrons in localized f-orbitals.[6]

This raises the more general question of the role of the two metals in the partial reduction of a mixed metal oxide system. For $VO_x$ particles on a $CeO_2(111)$ surface, photoelectron spectroscopy in agreement with density functional theory (DFT) demonstrated that vanadium becomes fully oxidized (+5 oxidation state), whereas reduced cerium (+3) is formed.[11] DFT calculations for crystalline $CeVO_4$ also found that the $Ce^{(+3)}{}_2O_3 \cdot V^{(+5)}{}_2O_5$ form with reduced Ce is more stable than $Ce^{(+4)}O_2 \cdot V^{(+4)}O_2$ with reduced V, that is, the extra electron prefers the Ce-4f states rather than the V-3d states.[12]

Here, we study three binary metal oxide gas-phase clusters, $Ce_mV_nO_o^+$, by infrared vibrational predissociation (IRVPD) spectroscopy in combination with DFT. Charged species are required for mass selection. In $CeVO_4^+$ (**1**), both metal atoms are fully oxidized. There is no doubt about the $Ce^{(+4)}O_2 \cdot V^{(+5)}O_2^+$ electronic structure with all Ce-4f and V-3d states empty. For the $CeV_2O_6^+$ species (**2**), which can also be written as $(CeVO_4)$-$(V^{(+5)}O_2^+)$, the same question arises as that for crystalline $CeVO_4$: Is the extra electron populating the Ce-4f or the V-3d states and does this lead to geometrically different isomers? Our DFT calculations show that this is indeed the case and that the measured IR spectra provide compelling evidence for electron localization in Ce-4f states. Also for the $Ce_2VO_5^+$ species (**3**), which can be written as $(CeVO_4)(Ce^{(+3)}O^+)$, we find that vanadium is in the +5 oxidation state, whereas both cerium atoms are in the +3 oxidation state.

This study does not only probe the relative reducibility of ceria versus vanadia, it also provides hints on the applicability of different DFT approaches to electronic structures with localized (Ce)-4f or (V)-3d states. For gas-phase oxide clusters, we can easily apply the more reliable hybrid functionals (see, e.g., ref 13), and this we do in the present study, whereas for solid materials,[14,15] use of hybrid functionals is more demanding, and the so-called DFT+U approach[16,17] is routinely applied.

Specifically, the IR spectra of **1**−**3** are measured by IRVPD spectroscopy. DFT with the B3LYP hybrid functional is employed to optimize the structures of energetically low-lying isomers of **1**−**3** and to calculate their linear IR spectra. The

**Special Issue:** Pavel Hobza Festschrift

**Received:** April 8, 2011
**Published:** May 03, 2011

  

assignment of the observed spectrum to a particular isomer with a given oxidation state of the metal atoms involved is based on the agreement between observed and predicted spectra together with the lowest-energy criterion. For comparison, DFT calculations are also made for the corresponding binary oxide clusters $M_mV_nO_o^+$ involving another redox-active oxide, M = Ti, and an inert oxide, M = Si, as models for vanadia supported by titania and silica, respectively.

Ce-containing clusters have not been spectroscopically studied in the gas phase up to now, but the reactivity of $Ce_mO_{2m}^+$ cations toward CO and small hydrocarbon molecules was studied mass spectrometrically and interpreted on the basis of DFT calculations.[18] IR spectra of small $Ce_mO_n^{+/0/-}$ $(m, n \leq 2)$ clusters in an Ar matrix have also been measured.[19] DFT calculations for mixed vanadia−ceria systems have been performed so far only on solid $CeVO_4$[12] and for $VO_n$ clusters on the $CeO_2(111)$ surface.[6,11,20]

## 2. EXPERIMENTAL DETAILS

IRVPD experiments are carried out using an ion trap/tandem mass spectrometer,[21,22] temporarily installed at the Free Electron Laser for Infrared eXperiments (FELIX) facility[23] at the FOM Institute Rijnhuizen (The Netherlands). The binary vanadium−cerium oxide cluster cations are generated by a 10 Hz dual laser vaporization source.[24] The plasma, containing vanadium and cerium atoms, is entrained in a pulse of 0.1% $O_2$ seeded in He carrier gas and expanded through a clustering channel. After passing through a 4 mm diameter skimmer the ions are collimated and translationally cooled in a buffer-gas-filled radio frequency (RF) decapole ion guide. Parent ions are mass-selected in a quadrupole mass filter, deflected by 90° in an electrostatic quadrupole deflector, and focused into a cryogenically cooled RF ring electrode ion trap. To allow for continuous ion loading, ion thermalization, and ion−He atom (Ne atom) complex formation, the trap is continuously filled with He (Ne) as a buffer gas at an ion trap temperature of 15 K (19 K for Ne). Rare-gas-tagged complexes are stabilized through three-body collisions.[25,26] Because the ion yields of **2**·He and **3**·He are too small, we use the corresponding Ne complexes for the IRVPD measurements. After filling the trap for 98 ms, all ions are extracted from the ion trap and focused both temporally and spatially into the center of the extraction region of an orthogonally mounted linear time-of-flight (TOF) mass spectrometer. Here, the ion packet can be irradiated with the IR laser pulse prior to the application of high-voltage pulses on the TOF electrodes and the subsequent measurement of the TOF mass spectrum.

IR spectra are obtained in the difference mode of operation (laser on−laser off) and recorded by monitoring all ion intensities simultaneously as the laser wavelength is scanned (50−70 measurements per wavelength step). FELIX is operated at a repetition rate of 5 Hz from 400 to 1200 $cm^{-1}$ with a bandwidth of ∼0.2% RMS of the central wavelength and average pulse energies of 10 mJ. The photodissociation cross section $\sigma$ is determined from the relative abundances of the parent and photofragment ions, $I_0$ and $I(\nu)$, and the frequency-dependent laser power $P(\nu)$ using $\sigma = -\ln[I(\nu)/I_0]/P(\nu)$.[27]

## 3. COMPUTATIONAL DETAILS

The TURBOMOLE 6.2 program is used for all calculations.[28] The B3LYP hybrid functional[29,30] is employed together with a triple-ζ valence basis set adjusted by g polarization functions for Ce atoms (TZVPP[31]). The binding energies between the ions and the rare gas atoms are calculated using the B3LYP+D(ispersion)[32] model. Structure optimizations use tight convergence criteria. Structures are optimized until Cartesian gradients are smaller than $1 \times 10^{-5}$ Hartree/Bohr and the energy change is smaller than $1 \times 10^{-6}$ Hartree. The SCF convergence criterion is $1 \times 10^{-7}$ Hartree for the energy and $1 \times 10^{-7}$ au for the RMS of the density. Open-shell singlet states for **3** are described by broken-symmetry solutions.[33,34] Harmonic vibrational frequencies are obtained from analytic second derivatives.[35] Zero-point vibrational energy contributions have been taken into account for the determination of relative energies. It is known that B3LYP vibrational frequencies are systematically too large (see, e.g., refs 36 and 37), and therefore, agreement with observed frequencies can be improved by scaling. Scaling accounts for both anharmonicities and systematic errors of the calculated harmonic force constants (calculated harmonic wave numbers are compared to observed fundamentals including anharmonicities). We use scaling parameters that were determined for small vanadium oxide cluster cations.[38] The vanadyl (V═O) modes are scaled by 0.9167, and all other modes are scaled by 0.9832. The simulated linear absorption spectra are derived from scaled harmonic frequencies and intensities. The resulting stick spectra are convoluted using a Gaussian line shape function with a width of 10 $cm^{-1}$ (fwhm) to account for the laser bandwidth.

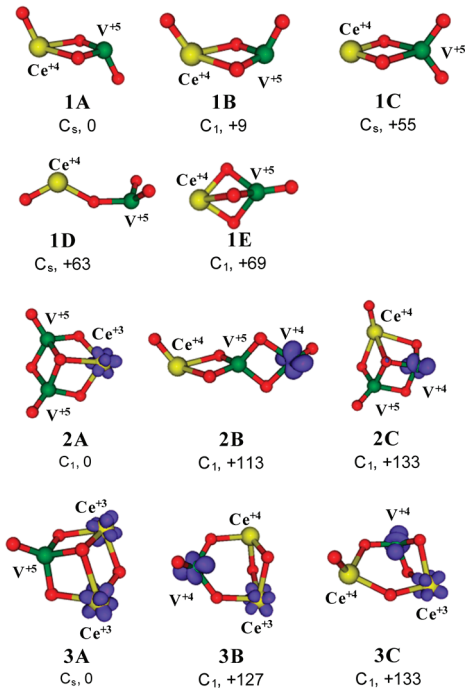


**Figure 1.** Optimized B3LYP/TZVPP structures and relative energies (in kJ/mol) of several low-lying isomers of $CeVO_4^+$ (**1**), $CeV_2O_6^+$ (**2**), and $Ce_2VO_5^+$ (**3**). (O red, V olive, Ce yellow). The oxidation state of each metal atom is specified. The purple spin density isosurface indicates electron localization on either Ce or V.

## 4. RESULTS

**4.1. Structures and Energies of Isomers.** The calculated relative energies (in kJ/mol), optimized structures, and spin densities of several low-lying isomers for species **1**, **2**, and **3** are shown in Figure 1 (see Table S1 (Supporting Information) for total electronic and zero-point vibrational energies). The lowest-energy isomer of **1** is characterized by a nearly planar, four-

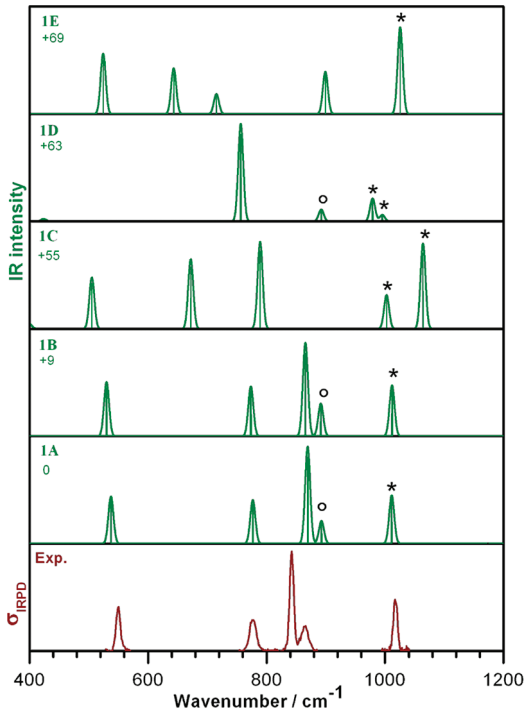


**Figure 2.** Comparison of experimental IRVPD spectra of He-tagged $CeVO_4^+$ (**1**·He, bottom row) to simulated B3LYP/TZVPP IR spectra of the isomers **1A**−**1E** (upper rows). V═O modes are marked with an asterisk, and Ce═O modes are marked with an open circle. Relative energies are given in kJ/mol.

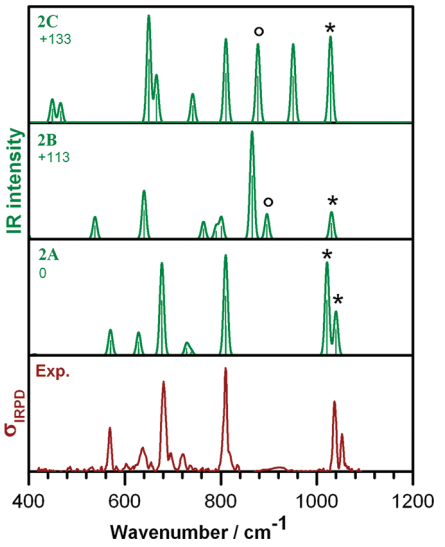


**Figure 3.** Comparison of experimental IRVPD spectra of Ne-tagged $CeV_2O_6^+$ (**2**·Ne, bottom row) to simulated B3LYP/TZVPP IR spectra of the isomers **2A**−**2C** (upper rows). V═O modes are marked with an asterisk, and Ce═O modes are marked with an open circle. Relative energies are given in kJ/mol.

membered M−$(O)_2$−M ring with two terminal M═O bonds in trans configuration (**1A** in Figure 1). It is similar to the structures previously reported for $Zr_2O_4$ or $V_2O_4^+$.[34,38,39] Both metal centers are fully oxidized ($Ce^{+4}$ and $V^{+5}$), resulting in a closed-shell $^1A'$ electronic ground state. The V═O and Ce═O bond lengths are 1.57 and 1.75 Å, respectively. Other isomers, including one with the terminal M═O bonds in cis configuration (**1B**), as well as scissor-like (**1C**), chain-like (**1D**), and tribridged (**1E**) structures, lie +9, +55, +63, and +69 kJ/mol, respectively, higher in energy than **1A**. The He atom binds preferentially to the V atom of **1A** (Figure S1, Supporting Information), that is, the positive charge center, with a binding energy of 13 kJ/mol. The structural parameters of **1A** and **1A**·He (Table S3, Supporting Information) are nearly identical.

The ground state of **2** is a $^2A$ state with a cage-like structure of $C_1$ symmetry featuring two V═O groups and a three-fold-coordinated Ce atom (**2A** in Figure 1). Chain-like (**2B**) and cage-like structures (**2C**) carrying single V═O and Ce═O subunits and the lowest-energy quartet state related to the $^2A$ ground state are predicted at +113, +133, and +297 kJ/mol, respectively. Structure **2A** is similar to the structure reported for $Zr_3O_6$[39] but is different from that of $V_3O_6^+$,[40] which prefers a **2B**-like structure. The spin density isosurface (Figure 1) shows that the unpaired electron in **2A** resides on the Ce atom, yielding oxidation states of $Ce^{+3}/V^{+5}/V^{+5}$, in contrast to the energetically higher-lying isomers **2B** and **2C**, which correspond to $Ce^{+4}/V^{+4}/V^{+5}$. In the messenger atom complex **2A**·Ne ($E_{ion-Ne}$ = 9.1 kJ/mol), the Ne atom prefers the low (three-fold)-coordinated Ce site, rather than the four-fold-coordinated V sites (see Figure S2, Supporting Information).

The cage-like structure **3A** (Figure 1) with $C_s$ symmetry is predicted to be the lowest-energy isomer for **3**. It has an open-shell $^1A'$ ground state in which the spins on the $Ce^{+3}$ sites are antiferromagnetically coupled. The corresponding $^3A'$ state (with parallel spins) is almost isoenergetic (+0.03 kJ/mol) with nearly identical structural parameters (Table S3, Supporting Information). The next two low-lying isomers are the bicyclic triplet species **3B** (+127 kJ/mol) and **3C** (+133 kJ/mol). All three isomers contain one terminal oxygen atom, either in a V═O (**3A**, **3B**) or in a Ce═O (**3C**) double bond, and exhibit different oxidation states, $Ce^{+3}/Ce^{+3}/V^{+5}$ (**3A**) or $Ce^{+3}/Ce^{+4}/V^{+4}$ (**3B**, **3C**). Attachment of Ne to **3A** leads to structure **3A**·Ne (Figure S3, Supporting Information), in which the Ne atom is located at a similar distance from all three metal atoms ($E_{ion-Ne}$ = 11 kJ/mol).

Summarizing, the present calculations predict ground-state structures for ions **1**−**3**, which are at least +55 kJ/mol more stable than other structural isomers. Whereas the electronic structure of **1** corresponds to fully oxidized metal centers ($Ce^{+4}/V^{+5}$), for the partially reduced species **2** and **3**, the most stable structures correspond exclusively to reduction of the Ce atoms ($Ce^{+3}$), whereas the $V^{+5}$ centers remain unaffected.

**4.2. Vibrational Spectra.** To test the computational predictions, the experimental IRVPD spectra of **1**·He, **2**·Ne, and **3**·Ne are compared with simulated IR absorption spectra of several low-lying isomers in Figures 2−4. Experimental peak positions are listed together with harmonic frequencies and intensities of the lowest-energy isomers in Table 1. The simulated B3LYP IR spectra of the bare ion and the corresponding rare gas complexes are nearly identical ($\leq \pm 5$ $cm^{-1}$), showing that the influence of the messenger atom on the IR absorptions is negligible (Figures S1−S3, Supporting Information). The same holds for the B3LYP-D IR spectra; however, the difference between the two models, without and with dispersion interaction, is slightly larger ($\leq \pm 8$ $cm^{-1}$).

Five absorption bands are observed at 1017, 866, 843, 776, and 551 $cm^{-1}$ in the IRVPD spectrum of **1**·He (Figure 2). The experimental spectrum shows excellent agreement with the simulated spectrum of the lowest-energy isomer **1A** both for band

positions and relative intensities. The spectra of isomers **1A** and **1B**, the cis/trans isomers, are predicted to be very similar. The separation and relative intensities of the 843 and 866 $cm^{-1}$ bands in the experimental spectrum (23 $cm^{-1}$, 1:0.25) are closer to those of the trans isomer **1A** (+24 $cm^{-1}$, 1:0.23) than those of the cis isomer **1B** (+26 $cm^{-1}$, 1:0.35), favoring an assignment to the trans isomer **1A**, which is calculated to be 9 kJ/mol lower in energy. The IR spectra of the energetically higher-lying scissor-like (**1C**), chain-like (**1D**), and tribridge (**1E**) structures (Figure 2) are markedly different from the experimental one, excluding them from the assignment. The two highest-energy IR bands of **1**·He are assigned to the V═O ($\nu_{exp}$ = 1017 $cm^{-1}$/$\nu_{calc}$ = 1011 $cm^{-1}$) and Ce═O (866/893) stretching modes. Due to the 1.7 higher mass of Ce compared to that of V, the Ce═O band is red-shifted relative to the vanadyl band, to a spectral region that overlaps with the M−$(O)_2$−M ring vibrations (∼400−900 $cm^{-1}$),[40] leading to substantial coupling between the Ce═O and the antisymmetric M−O ring stretching mode (843/869), in this particular case. The symmetric ring stretching (776/777) and breathing (551/537) modes are found at lower energies.

The IRVPD spectrum of **2**·Ne (Figure 3) shows seven IR bands at 1052, 1037, 810, 720, 681, 638, and 569 $cm^{-1}$. Excellent agreement is found with the simulated IR spectrum of the lowest-energy isomer **2A**. The doublet (1052 and 1037 $cm^{-1}$) observed above 1000 $cm^{-1}$ is characteristic for structure **2A** because it unambiguously identifies the presence of two vanadyl groups, which yield a symmetric and an antisymmetric combination of the two V═O stretching modes (1040 and 1021 $cm^{-1}$). In contrast, isomers **2B** and **2C** exhibit a single V═O plus one Ce═O group. Consequently only a single band at 1031 $cm^{-1}$ (1028 $cm^{-1}$) is predicted for **2B** (**2C**). The Ce═O stretching modes at 896 (**2B**) and 877 $cm^{-1}$ (**2C**) lie in a spectral region where no significant absorption is found in the experiment. The features below 800 $cm^{-1}$ are attributed to stretching and bending vibrations involving the doubly coordinated O atoms.

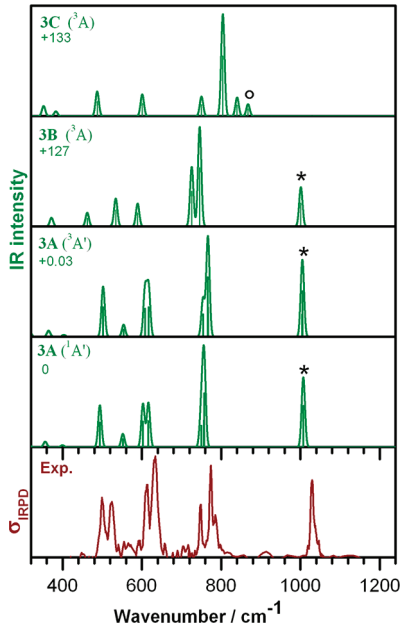


**Figure 4.** Comparison of experimental IRVPD spectra of Ne-tagged $Ce_2VO_5^+$ (**3**·Ne, bottom row) to simulated B3LYP/TZVPP IR spectra of the isomers **3A**−**3C** (upper rows). V═O modes are marked with an asterisk, and Ce═O modes are marked with an open circle. Relative energies are given in kJ/mol.

The IRVPD spectrum of **3**·Ne is shown in the bottom row of Figure 4. Seven peaks are observed at 1029, 774, 748, 634, 612, 524, and 499 $cm^{-1}$. The spectrum of the $^1$A′ ground state reproduces six of these bands (1005, 767, 754, 617, 608, and 502 $cm^{-1}$) satisfactorily and also accounts for the weak absorption band observed at ∼560 $cm^{-1}$ (554 $cm^{-1}$). The experimentally observed bands are assigned (in descending order with respect to energy) to one V═O stretching mode, three O−V−O stretching modes involving the doubly coordinated O atoms adjacent to the vanadium atom, as well as two more delocalized ring deformation modes, leaving the 524 $cm^{-1}$ band unassigned. Our initial assumption that this band may be attributed to the nearly isoenergetic $^3$A′ state is not confirmed by the calculations, which yield nearly identical vibrational frequencies for the $^1$A′ and $^3$A′ states (Figure 4 and Table S1, Supporting Information). We then considered different binding sites of the Ne atom to **3A**, but only a weak dependence of the binding site on the IR band positions was found (Figure S3, Supporting Information). Summarizing, we find the best agreement of the experimental spectrum of **3**·Ne with the cage-like structure **3A** corresponding to oxidation states of $Ce^{+3}/Ce^{+3}/V^{+5}$. Both quasi-degenerate states ($^3$A′ and $^1$A′) contribute to the IR spectrum but cannot be differentiated due to their nearly identical IR spectra.

The spectra of the energetically higher-lying isomers **3B** (+127 kJ/mol) and **3C** (+133 kJ/mol) should lie too high in energy to be probed in the experiment, and their simulated IR spectra also fit less well with the experiment compared to the spectrum of **3A**. We conclude that structures **3B** and **3C**, which contain a $V^{+4}$ center, are not observed.

## 5. DISCUSSION

The good agreement between the experimental IRVPD spectra and the simulated IR spectra of the lowest-energy structure for the three systems **1**−**3** considered here shows that the B3LYP/TZVPP calculations yield reliable relative energies and structures and, on this basis, reproduce the vibrational

**Table 1. Experimental IRVPD Peak Positions ($cm^{-1}$), B3LYP/TZVPP Scaled Harmonic Frequencies ($cm^{-1}$), and Intensities (km/mol) of the Lowest-Energy Isomers of 1−3 Clusters**[a]

| ion | exp./theory[b] | vibrational frequencies |
|---|---|---|
| **1**·He | experiment | 1017, 866, 843, 776, 551 |
| **1A** | $^1$A′, $C_s$ | 1011(a′,187), 893(a′,88), 869(a′,375), 777(a′′,169), 537(a′,182) |
| **2**·Ne | experiment | 1052, 1037, 810, 720, 681, 638, 569 |
| **2A** | $^2$A, $C_1$ | 1040(a,185), 1021(a,392), 810(a,422), 737(a,23), 729(a,51), 677(a,389), 629(a,96), 570(a,107) |
| **3**·Ne | experiment | 1029, 774, 748, 634, 612, 524, 499 |
| **3A** | $^1$A′, $C_s$ | 1005(a′,319), 767 (a′′,416), 754 (a′,158), 617(a′,207), 608(a′′,198), 554(a′,49), 502(a′,208) |

[a] Only vibrational modes with scaled harmonic frequencies above 400 $cm^{-1}$ are shown. See Table S3 (Supporting Information) for a complete list of harmonic frequencies of all calculated species. [b] Electronic state and symmetry group are given.

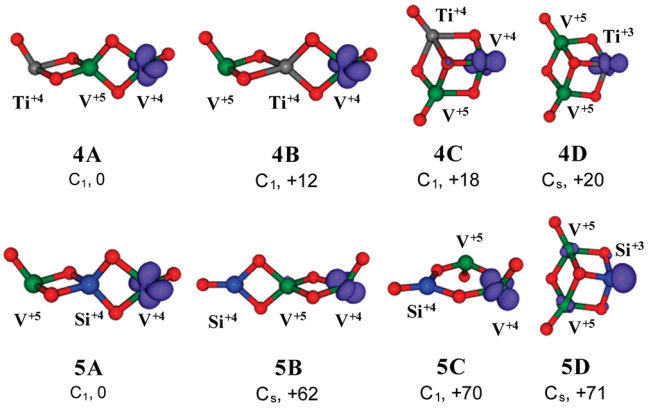


**Figure 5.** Optimized B3LYP/TZVPP structures and relative energies (in kJ/mol) of four low-lying isomers of $TiV_2O_6^+$ (**4A**−**4D**) and $SiV_2O_6^+$ (**5A**−**5D**). (O red, V olive, Ti dark gray, Si blue). The oxidation state of each metal atom is specified. The purple spin density isosurface indicates electron localization on either Ti/Si or V.

properties of Ce-containing oxide clusters. In each case, the experiment confirms the predicted structures for species **1** ($Ce^{+4}/V^{+5}$), **2** ($Ce^{+3}/V^{+5}/V^{+5}$), and **3** ($Ce^{+3}/Ce^{+3}/V^{+5}$). Specifically, we find that in our gas-phase binary metal oxide clusters, the electron distribution leading to $Ce(f^1)^{+3}/V^{+5}$ is more stable than $Ce^{+4}/V(d^1)^{+4}$, which is consistent with previous experimental[41] and DFT+U results[12] for crystalline CeVO4, as well as with the preferential reducibility of cerium oxides over vanadium oxides reported previously.[15,42,43] It also agrees with a joint computational and surface science study[11] in which a solid ceria film was shown to stabilize vanadium oxide adspecies always in their highest oxidation state +5, whereas cerium was partially reduced.

This $Ce(f^1)^{+3}/V^{+5}$ preference is in contrast to the $Ce^{+4}/V(d^1)^{+4}$ preference inferred from both of the reduction potentials in aqueous solution[44] (1.3−1.7 eV for $Ce^{+4}$ depending on pH and 1.0 eV for $V^{+5}$ in $VO_2^+$) and the heats of formation for the bulk oxides.[10,45,46] The latter yield endothermicity ($\Delta H°_{298}$= 1.0−1.3 eV) for the reaction

$$CeO_2 + VO_2 \rightarrow \frac{1}{2}Ce_2O_3 + \frac{1}{2}V_2O_5$$

DFT+U calculations also show that the above reaction is unfavorable ($\Delta H°_0$ = 0.25 eV), whereas the reaction leading to bulk $Ce(f^1)VO_4$

$$CeO_2 + VO_2 \rightarrow CeVO_4$$

is strongly exothermic, $\Delta H°_0 = -1.53$ eV.[12]

What is different in $CeVO_4$ compared to $Ce_2O_3 + V_2O_5$ is the coordination of the ions and the average distance to the oxygen ligands, which determine the splitting, and hence the stability, of f and d states, respectively. In $Ce_2O_3$, Ce is coordinated to seven O ions (average distance of 250 pm), whereas in $CeVO_4$, it is coordinated to eight O (distance of 248 pm).[12] The vanadium coordination in $V_2O_5$ is 5 (average distance of 186 pm), and in $CeVO_4$, it is 4 (V−O distance of 171 pm), whereas it is 6 in $VO_2$ (average distance of 193 pm).[12] In $CeVO_4$, the vanadium coordination is very far from the optimum values for $V^{+4}$, whereas the coordination environment for Ce in $CeVO_4$ is similar to that in $Ce_2O_3$. We conclude that the $Ce^{+4}/V(d^1)^{+4}$ pair is more stable when the coordination numbers are high, as in the bulk solids or in aqueous solution, whereas a low coordination of vanadium as found in $CeVO_4$ or for vanadia species on ceria supports favors the $Ce^{+3}(f^1)/V^{+5}$ pair. In the gas-phase clusters studied here, the coordination numbers of both Ce and V are small, and in the most stable isomers, **2A** and **3A**, occupation of d states on four-fold-coordinated vanadium is avoided, as in $CeVO_4$.

For comparison with other typical support materials like titania and silica, we performed calculations on additional binary metal oxide clusters, replacing Ce with Ti and Si. These DFT calculations predict that, in contrast to the cage-like structure of $CeV_2O_6^+$ (**2A**), the binary metal oxide clusters $TiV_2O_6^+$ (**4**) and $SiV_2O_6^+$ (**5**) prefer chain-like structures (Figure 5). Among the cage-like $MV_2O_6^+$ structures (M = Ti, Ce), **4C** with $Ti^{+4}/V^{+4}$ is slightly (1.6 kJ/mol) more stable that **4D** with $Ti^{+3}/V^{+5}$, whereas **2C** with $Ce^{+4}/V^{+4}$ is 133 kJ/mol less stable than **2A** with $Ce^{+3}/V^{+5}$ (Figure 1). This suggests that the reduction of $Ti^{+4}$ to $Ti^{+3}$ is competitive with that of $V^{+5}$ to $V^{+4}$. Comparing the $Ce^{+4}/V^{+4}$ and $Ti^{+4}/V^{+4}$ structures, the chain-like isomers **2B** and **4A**, respectively, are 20 and 18 kJ/mol more stable than the cage-like isomers with the same electron localization, **2C** and **4C**, respectively. They both have the $V^{+5}$ species with the positive charge in the central four-fold-coordinated site. Only because of the unusual stabilization of vanadia in its highest oxidation state by cerium oxide does the cage-like structure **2A** with the $Ce^{+3}/V^{+5}$ pair become the most stable isomer for $CeV_2O_6^+$. For Si, reduction to $Si^{+3}$ is generally very unlikely, and structure **5D** is 71 kJ/mol less favorable than **5A**. Furthermore, the chain-like isomer **5A** with $Si^{+4}$ in the middle is much more stable (62 kJ/mol) than the one with $Si^{+4}$ in a terminal position (**5B**) because, in contrast to Ti, Si does not easily form terminal Si=O double bonds. A previous DFT study[20] also found that the structure of $VO_x$ species supported on ceria is different from that supported on titania and also that their redox chemistry is different.

## 6. SUMMARY AND CONCLUSIONS

The experimental IRVPD spectra of the cerium−vanadium oxide cluster cations **1**−**3** are well-reproduced by the simulated IR spectra of the lowest-energy isomer predicted by B3LYP/TZVPP calculations, confirming that the B3LYP hybrid functional properly localizes electrons in the gas-phase Ce-containing binary metal oxide clusters studied here. Experimental evidence is found for the predicted larger stability of $Ce^{+3}/V^{+5}$ compared to that of $Ce^{+4}/V^{+4}$. We find crucial differences with respect to the relative reducibility in different binary metal−vanadium oxide clusters. Whereas in the vanadia−ceria clusters $Ce^{+4}$ is easily reduced to $Ce^{+3}$, stabilizing the $V^{+5}$ center, in vanadia−titania clusters, reduction of $Ti^{+4}$ to $Ti^{+3}$ is competitive with that of $V^{+5}$ to $V^{+4}$, and in vanadia−silica clusters, $Si^{+4}$ cannot be reduced. The present results confirm that an easily reducible support material, like ceria, may serve as an electron acceptor for the electron transferred to the active site in the rate-determining step.[6−8] Hence, IRVPD spectroscopy on electronically tailored binary metal oxide clusters, combined with properly chosen quantum chemical calculations, may contribute to the understanding of complex solid catalysts.

## ■ ASSOCIATED CONTENT

**Supporting Information.** Figures S1−S3: B3LYP and B3LYP+D IR spectra and structures of the lowest-energy isomers of $CeVO_4^+$, $CeV_2O_6^+$, and $Ce_2VO_5^+$ with and without a rare gas atom. Tables S1 and S2: B3LYP and B3LYP+D total

electronic energies, zero-point vibrational energies, relative energies, binding energies, and a share of dispersion on the binding energy of energetically low-lying isomers. Table S3: Cartesian coordinates and unscaled harmonic frequencies and intensities for all structures. This material is available free of charge via the Internet at http://pubs.acs.org.

## AUTHOR INFORMATION

### Corresponding Author

* E-mail: asmis@fhi-berlin.mpg.de. Fax: +49-30-8413-5603. Tel: +49-30-8413-5735. (K.R.A.); E-mail: Peter.Lievens@fys.kuleuven.be. Fax: +32-16-327983. Tel: +32-16-327207. (P.L.); E-mail: js@chemie.hu-berlin.de. Fax: +49-30-2093-7136. Tel:+49-30-2093-7135. (J.S.).

## ACKNOWLEDGMENT

We would like to thank the Stichting voor Fundamenteel Onderzoek der Materie (FOM) for beam time at FELIX and the FELIX staff for support and assistance. This research is funded by the German Research Foundation (Center of Colloborative Research 546), by the Fund for Scientific Research - Flanders (FWO), the K.U.Leuven Research Council (BOF, GOA, and IDO programs), and the European Community's Seventh Framework Programme (FP7/2007-2013) Grant 226716. L.J. thanks the Alexander von Humboldt Foundation for a post doctoral scholarship, and P.C. thanks the Agency for Innovation by Science and Technology in Flanders (IWT) for a doctoral scholarship.

## REFERENCES

(1) Weckhuysen, B. M.; Keller, D. E. *Catal. Today* **2003**, *78*, 25.
(2) Wachs, I. E. *Catal. Today* **2005**, *100*, 79.
(3) Bañares, M. A. *Catal. Today* **1999**, *51*, 319.
(4) Khodakov, A.; Olthof, B.; Bell, A. T.; Iglesia, E. *J. Catal.* **1999**, *181*, 205.
(5) Dinse, A.; Frank, B.; Hess, C.; Habel, D.; Schomacker, R. *J. Mol. Catal. A: Chem.* **2008**, *289*, 28.
(6) Ganduglia-Pirovano, M. V.; Popa, C.; Sauer, J.; Abbott, H.; Uhl, A.; Baron, M.; Stacchiola, D.; Bondarchuk, O.; Shaikhutdinov, S.; Freund, H. J. *J. Am. Chem. Soc.* **2010**, *132*, 2345.
(7) Döbler, J.; Pritzsche, M.; Sauer, J. *J. Am. Chem. Soc.* **2005**, *127*, 10861.
(8) Rozanska, X.; Fortrie, R.; Sauer, J. *J. Phys. Chem. C* **2007**, *111*, 6041.
(9) Daniell, W.; Ponchel, A.; Kuba, S.; Anderle, F.; Weingand, T.; Gregory, D. H.; Knozinger, H. *Top. Catal.* **2002**, *20*, 65.
(10) Trovarelli, A. *Catalysis by Ceria and Related Materials*; Imperial College Press: London, 2002; Vol. 2.
(11) Baron, M.; Abbott, H.; Bondarchuk, O.; Stacchiola, D.; Uhl, A.; Shaikhutdinov, S.; Freund, H. J.; Popa, C.; Ganduglia-Pirovano, M. V.; Sauer, J. *Angew. Chem., Int. Ed.* **2009**, *48*, 8006.
(12) Da Silva, J. L. F.; Ganduglia-Pirovano, M. V.; Sauer, J. *Phys. Rev. B* **2007**, *76*, 125117.
(13) Asmis, K. R.; Santambrogio, G.; Brümmer, M.; Sauer, J. *Angew. Chem.* **2005**, *117*, 3182.
(14) Cora, F.; Alfredsson, M.; Mallia, G.; Middlemiss, D. S.; Mackrodt, W. C.; Dovesi, R.; Orlando, R. *Struct. Bonding (Berlin, Ger.)* **2004**, *113*, 171.
(15) Ganduglia-Pirovano, M. V.; Hofmann, A.; Sauer, J. *Surf. Sci. Rep.* **2007**, *62*, 219.
(16) Anisimov, V. I.; Zaanen, J.; Andersen, O. K. *Phys. Rev. B* **1991**, *44*, 943.
(17) Liechtenstein, A. I.; Anisimov, V. I.; Zaanen, J. *Phys. Rev. B* **1995**, *52*, R5467.
(18) Wu, X.-N.; Zhao, Y.-X.; Xue, W.; Wang, Z.-C.; He, S.-G.; Ding, X.-L. *Phys. Chem. Chem. Phys.* **2010**, *12*, 3984.
(19) Willson, S. P.; Andrews, L. *J. Phys. Chem. A* **1999**, *103*, 3171.
(20) Shapovalov, V.; Metiu, H. *J. Phys. Chem. C* **2007**, *111*, 14179.
(21) Goebbert, D. J.; Meijer, G.; Asmis, K. R. *AIP Conf. Proc.* **2009**, *1104*, 22.
(22) Goebbert, D. J.; Wende, T.; Bergmann, R.; Meijer, G.; Asmis, K. R. *J. Phys. Chem. A* **2009**, *113*, 5874.
(23) Oepts, D.; van der Meer, A. F. G.; van Amersfoort, P. W. *Infrared Phys. Technol.* **1995**, *36*, 297.
(24) Bouwen, W.; Thoen, P.; Vanhoutte, F.; Bouckaert, S.; Despa, F.; Weidele, H.; Silverans, R. E.; Lievens, P. *Rev. Sci. Instrum.* **2000**, *71*, 54.
(25) Brümmer, M.; Kaposta, C.; Santambrogio, G.; Asmis, K. R. *J. Chem. Phys.* **2003**, *119*, 12700.
(26) Lin, L.; Claes, P.; Höltzl, T.; Janssens, E.; Wende, T.; Bergmann, R.; Santambrogio, G.; Meijer, G.; Asmis, K. R.; Nguyen, M. T.; Lievens, P. *Phys. Chem. Chem. Phys.* **2010**, *12*, 13907.
(27) Oomens, J.; Tielens, A. G. G. M.; Sartakov, B.; von Helden, G.; Meijer, G. *Astrophys. J.* **2003**, *591*, 968.
(28) *TURBOMOLE V6.2*; a development of University of Karlsruhe and Forschungszentrum Karlsruhe GmbH, 1989−2007, TURBOMOLE GmbH, since 2007; available from http://www.turbomole.com (2010).
(29) Becke, A. D. *J. Chem. Phys.* **1993**, *98*, 5648.
(30) Lee, C.; Yang, W.; Parr, R. G. *Phys. Rev. B* **1988**, *37*, 785.
(31) Weigend, F.; Ahlrichs, R. *Phys. Chem. Chem. Phys.* **2005**, *7*, 3297.
(32) Grimme, S. *J. Comput. Chem.* **2006**, *27*, 1787.
(33) Noodleman, L. *J. Chem. Phys.* **1981**, *74*, 5737.
(34) Pykavy, M.; van Wüllen, C.; Sauer, J. *J. Chem. Phys.* **2004**, *120*, 4207.
(35) Deglmann, P.; Furche, F.; Ahlrichs, R. *Chem. Phys. Lett.* **2002**, *362*, 511.
(36) Halls, M. D.; Velkovski, J.; Schlegel, H. B. *Theor. Chem. Acc.* **2001**, *105*, 413.
(37) Scott, A. P.; Radom, L. *J. Phys. Chem.* **1996**, *100*, 16502.
(38) Asmis, K. R.; Meijer, G.; Brümmer, M.; Kaposta, C.; Santambrogio, G.; Wöste, L.; Sauer, J. *J. Chem. Phys.* **2004**, *120*, 6461.
(39) von Helden, G.; Kirilyuk, A.; van Heijnsbergen, D.; Sartakov, B.; Duncan, M. A.; Meijer, G. *Chem. Phys.* **2000**, *262*, 31.
(40) Asmis, K. R.; Sauer, J. *Mass Spectrom. Rev.* **2007**, *26*, 542.
(41) Reidy, R. F.; Swider, K. E. *J. Am. Ceram. Soc.* **1995**, *78*, 1121.
(42) Reddy, B. M.; Khan, A.; Yamada, Y.; Kobayashi, T.; Loridant, S.; Volta, J. C. *J. Chem. Phys. B* **2003**, *107*, 5162.
(43) Martinez-Huerta, M. V.; Coronado, J. M.; Fernandez-Garcia, M.; Iglesias-Juez, A.; Deo, G.; Fierro, J. L. G.; Banares, M. A. *J. Catal.* **2004**, *225*, 240.
(44) Cotton, F. A.; Wilkinson, G. *Advanced Inorganic Chemistry*; Interscience Publishers: New York, 1962.
(45) Brückner, W.; Oppermann, H.; Reichel, W.; Terukow, J. I.; Tschudnowski, F. A.; Wolf, E. *Vanadiumoxide — Darstellung, Eigenschaften, Anwendungen*; Akademie-Verlag: Berlin, Germany, 1983.
(46) Zinkevich, M.; Djurovic, D.; Aldinger, F. *Solid State Ionics* **2006**, *177*, 989.